

# Microwave-assisted method for preparation of Sb-doped ZnO nanostructures and their photocatalytic activity

Amir Omid · Aziz Habibi-Yangjeh

Received: 17 March 2013 / Accepted: 17 July 2013 / Published online: 25 July 2013  
© Iranian Chemical Society 2013

**Abstract** Nanostructures of Sb-doped ZnO with 0.00, 0.03, 0.06, 0.10 and 0.15 mol fractions of  $\text{Sb}^{+3}$  ions were prepared by a one-pot method in water under microwave irradiation for 5 min. Powder X-ray diffraction studies display that the nanostructures are excellently crystallized in the form of Wurtzite hexagonal crystalline phase and doping  $\text{Sb}^{+3}$  ions does not change structure of ZnO. Moreover, size of the nanostructures decreases with increasing mole fraction of  $\text{Sb}^{+3}$  ions. Scanning electron microscopy and transmission electron microscopy images show that morphology and size of the nanostructures are changing with mole fraction of the dopant. In Fourier transform infrared spectra, intensity of the characteristic peak corresponding to Sb–O bond gradually increases with mole fraction of  $\text{Sb}^{+3}$  ions. UV–vis diffuse reflectance spectra of the nanostructures are similar to each other and they have a maximum of about 357 nm. Photocatalytic activity of the nanostructures was investigated by degradation of methylene blue under UV irradiation. For the nanostructures with 0.10 mol fraction of  $\text{Sb}^{+3}$  ions, the degradation rate constant increases nearly two times relative to pure ZnO. In addition, influence of various operational parameters on the degradation activity was investigated and the results were discussed.

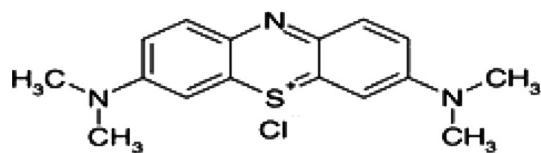
**Keywords** Sb-doped ZnO · Microwave irradiation · Nanostructures · Methylene blue

## Introduction

Semiconductor nanomaterials have been extensively studied in the past decade due to their vital applications in numerous technologies such as microelectronics, electro-optics, nonlinear optics, light energy conversion, photocatalysis and biological fluorescence labeling [1–5]. These nanomaterials present novel properties because of larger number of surface atoms and three-dimensional confinement of their electrons. Controlled preparation of the nanomaterials has attracted much attention, as a result of their fundamental shape and size-dependent activities. Among various methods that have been applied for preparation of these nanomaterials, solution-based approaches are appealing due to their low cost, high efficiency, and potential for scale-up [6, 7]. However, in these methods, using different templates will increase the reaction complexity, cause impurity in the products and disadvantageous from the view point of green chemistry. Thus, development of facile, effective, and template-free approaches for the controlled preparation of the materials is highly desirable.

Zinc oxide, as a wide band gap semiconductor, has been studied extensively in the past decade due to its fundamental and technological importance [8–11]. Its many attractive properties, such as wide band gap (3.37 eV), large exciton binding energy, excellent chemical stability, high photosensitivity, nontoxicity and low cost suggest a great deal of possible practical applications [12, 13]. Therefore, ZnO is one of the most important materials and its applications are expanding continuously. Many studies have been demonstrated that doping of ZnO with appropriate cations can remarkably affect its properties [14–16]. Recently, much attention has been paid to prepare Sb-doped ZnO nanomaterials because of possible applications

A. Omid · A. Habibi-Yangjeh (✉)  
Department of Chemistry, Faculty of Science, University of Mohaghegh Ardabili, P.O. Box 179, Ardabil, Iran  
e-mail: ahabibi@uma.ac.ir



**Scheme 1** Chemical structures for methylene blue (MB)

in various technologies [17–22]. However, the preparation methods have long reaction times, harmful chemicals, high temperatures, and complicate equipments. Therefore, it is highly desirable to prepare the nanomaterials using green, template-free and short time methods under mild conditions. Moreover, photocatalytic activity of Sb-doped ZnO nanomaterials for degradation of various organic pollutants very rarely has been studied [23, 24].

Compared with conventional methods, microwave preparation method has the advantages of short reaction time, small particle size, narrow particle size distribution and high purity [25]. This method is based on interaction of molecules in reaction mixture with electromagnetic waves. Dielectric heating is created by interaction of dipole moments of the molecules with the radiation [26]. Hence, microwave irradiation method has shown very rapid growth in its application to materials science due to its unique reaction effects such as rapid volumetric heating and the consequent dramatic increase in reaction rates [25, 27–29].

In the present paper, a one-pot microwave-assisted method was applied for preparation of Sb-doped ZnO nanostructures in water at 5 min. Moreover, influence of various operational parameters such as mole fraction of  $\text{Sb}^{+3}$  ions, irradiation time, calcination temperature, catalyst weight and pH of solution on photodegradation of methylene blue (MB) with chemical structure shown in Scheme 1 under UV irradiation was studied and the results were discussed.

## Materials and methods

### Materials

Zinc acetate ( $\text{Zn}(\text{CH}_3\text{COO})_2 \cdot 2\text{H}_2\text{O}$ , extra pure), antimony chloride ( $\text{SbCl}_3$ , extra pure), sodium hydroxide ( $\text{NaOH}$ ), MB and absolute ethanol were obtained from Merck and employed without further purification. Double distilled water was used for the experiments.

### Instruments

A domestic microwave oven (2.45 GHz and 1,000 W) was used for preparation of the nanostructures. X-ray

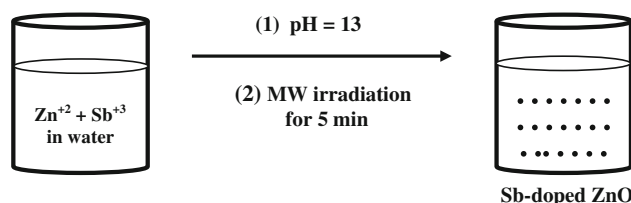
diffraction (XRD) patterns were recorded on a Philips Xpert X-ray diffractometer with  $\text{Cu K}\alpha$  radiation ( $\lambda = 0.15406 \text{ nm}$ ), employing scanning rate of  $0.04^\circ/\text{s}$  in  $2\theta$  range from  $20^\circ$  to  $80^\circ$ . Diffuse reflectance spectra (DRS) were recorded by a Scinco 4100 apparatus. Surface morphology and distribution of particles were studied via LEO 1430VP scanning electron microscopy (SEM), using an accelerating voltage of 15 kV. The samples used for SEM observations mounted on an aluminum support using a double adhesive tape coated with a thin layer of gold and palladium. Transmission electron microscope (TEM) measurements were performed on a Philips EM 208 with an acceleration voltage of 100 kV. The samples were prepared by dropping a diluted solution of nanostructures in ethanol on a carbon-coated copper grid and slowly drying in air. The Sb-doping content of the samples was determined by inductively coupled plasma model ICP-OES 730. Fourier transform-infrared (FT-IR) spectra were obtained using Perkin Elmer Spectrum RX I apparatus. The pH of the solutions was measured by Metrohm digital pH meter of model 691.

### Preparation of the nanostructures

For preparation of the nanostructures with 0.10 mol fraction of  $\text{Sb}^{+3}$ , zinc acetate (3.9508 g) and antimony chloride (0.4562 g) were dissolved in 100 ml of distilled water under stirring at room temperature. Then, aqueous solution of  $\text{NaOH}$  (5 M) was added dropwise into the solution under stirring at room temperature until pH of the solution reached to 13. The milky suspension was irradiated in air for 5 min with 55 % of output. The formed suspension was centrifuged to get the precipitate out and washed two times with double distilled water and ethanol, respectively, to remove the unreacted reagents and dried in an oven at  $60^\circ \text{C}$  for 24 h. The schematic diagram for preparation of the nanostructures has been illustrated in Scheme 2.

### Photocatalysis experiments

Photocatalysis experiments were performed in a cylindrical Pyrex reactor with about 400 ml capacity. The reactor provided with water circulation arrangement to maintain



**Scheme 2** The schematic process for preparation of Sb-doped ZnO under microwave irradiation

temperature at 25 °C. The solution was magnetically stirred and continuously aerated by a pump to provide oxygen and complete mixing of the reaction solution. A UV Osram lamp with 125 W was used as UV source. The lamp was fitted on the top of the reactor. Prior to illumination, a suspension containing 0.1 g of the nanostructures and 250 ml of MB ( $2.75 \times 10^{-5}$  M) was continuously stirred in dark for 30 min to attain adsorption equilibrium. Samples were taken from the reactor at regular intervals and centrifuged to remove the photocatalyst before analysis by spectrophotometer at 664 nm corresponding to maximum absorption wavelength of MB.

## Results and discussion

XRD patterns of Sb-doped ZnO nanostructures with various mole fractions of  $\text{Sb}^{+3}$  are shown in Fig. 1. As can be seen, the pure ZnO has Wurtzite hexagonal crystalline phase (JCPDS file no. 36-1451) and no peaks attributable to possible impurities are observed [30]. The Sb-doped ZnO nanostructures have XRD patterns similar to the pure ZnO and there are no characteristic peaks for separate phases of ZnO and  $\text{Sb}_2\text{O}_3$ . The average particle sizes,  $D$ , were calculated by Scherer's equation [31],  $D = K\lambda / (B \cos \theta)$  where  $\lambda$  is wavelength of X-ray radiation (0.15406 nm),  $K$  is Scherer's constant ( $K = 0.9$ ),  $\theta$  is characteristic X-ray radiation ( $2\theta = 36.35^\circ$ ) and  $B$  is full-width-at-half-maximum of (101) plane (in radians). Average particle sizes of the nanostructures with 0.00, 0.03, 0.06, 0.10 and 0.15 mol fractions of  $\text{Sb}^{+3}$  ions are about 21, 14, 9, 7 and 6 nm, respectively. As can

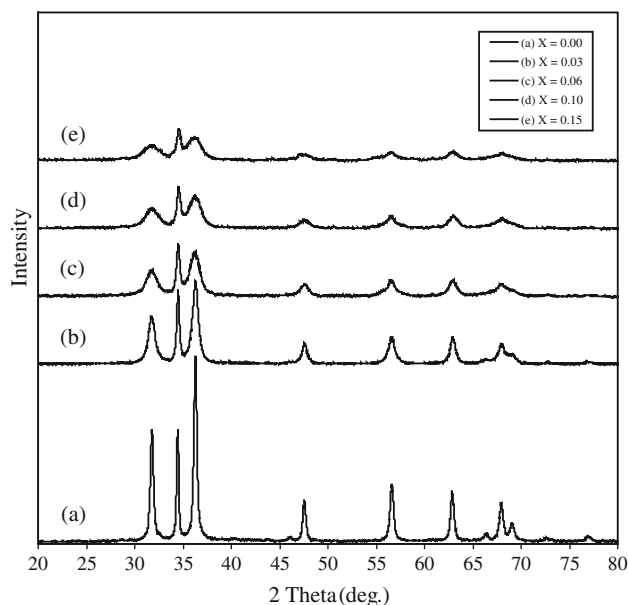


**Fig. 1** XRD patterns for Sb-doped ZnO nanostructures with various mole fractions of  $\text{Sb}^{+3}$  ions

be seen, the particle sizes systematically decrease with increasing mole fraction of  $\text{Sb}^{+3}$  ions. Segregation of antimony oxide on the grain boundary of ZnO can hinder the growth of it and hence size of the doped nanostructures decreases with increasing mole fraction of the dopant.

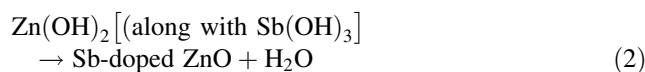
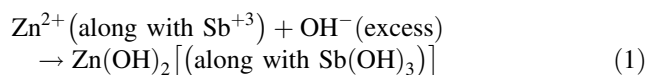
In Fig. 2, SEM images of the nanostructures with various mole fractions of  $\text{Sb}^{+3}$  ions were shown. It is evident that morphology of the pure ZnO is mainly plates with various sizes. The SEM images show that with increasing mole fraction of  $\text{Sb}^{+3}$  ions, morphology of the nanostructures is changing. As can be seen, size of the nanostructures obtained by SEM images is different from XRD calculated sizes; because, the nano-sized particles tend to aggregate into larger sized particles. That is to say the XRD estimated values are the size of single particles while SEM images show the agglomerates particles [32]. Similar results have been previously reported for different nanomaterials [32–34].

Figure 3 shows TEM images for the pure and Sb-doped ZnO nanostructures with 0.1 mol fraction of the dopant. It is clear that the nanostructures consist of particles with various sizes. The calculated particle sizes with appropriate homemade software for the pure and Sb-doped ZnO nanostructures are in the range of 11–42 and 5–26 nm, respectively. As can be clearly seen, with doping of  $\text{Sb}^{+3}$  ions, the size of the nanostructures decreases.

DRS of the nanostructures were obtained and the results are shown in Fig. 4. The pure ZnO with absorption maxima at 357 nm shows blue shift relative to bulk ZnO with absorption at 384 nm that can be attributed to quantum confinement effect of the nanocrystalline ZnO [35]. It can be seen that  $\text{Sb}^{+3}$  doping has a slight influence on absorption spectrum of the pure ZnO.

FT-IR spectra for the nanostructures with various mole fractions of  $\text{Sb}^{+3}$  ions are shown in Fig. 5. The broad absorption bands in range of  $2,800\text{--}3,600\text{ cm}^{-1}$  are corresponding to O–H stretching vibration of adsorbed water on the nanostructures. The peak about at  $570\text{ cm}^{-1}$  is related to Zn–O stretching mode [36]. Moreover, the peak at  $690\text{ cm}^{-1}$  is corresponding to Sb–O stretching vibration [37]. As can be seen, with increasing mole fraction of  $\text{Sb}^{+3}$  ions, intensity of the characteristic peak corresponding to Sb–O bond gradually increases.

A possible formation mechanism for Sb-doped ZnO nanostructures may be expressed by the following equations:



The ICP analysis was applied to determine the Sb-doping content. The measured values of the molar ratio of Sb to Zn in the nanostructures with 0.03, 0.06, 0.10 and

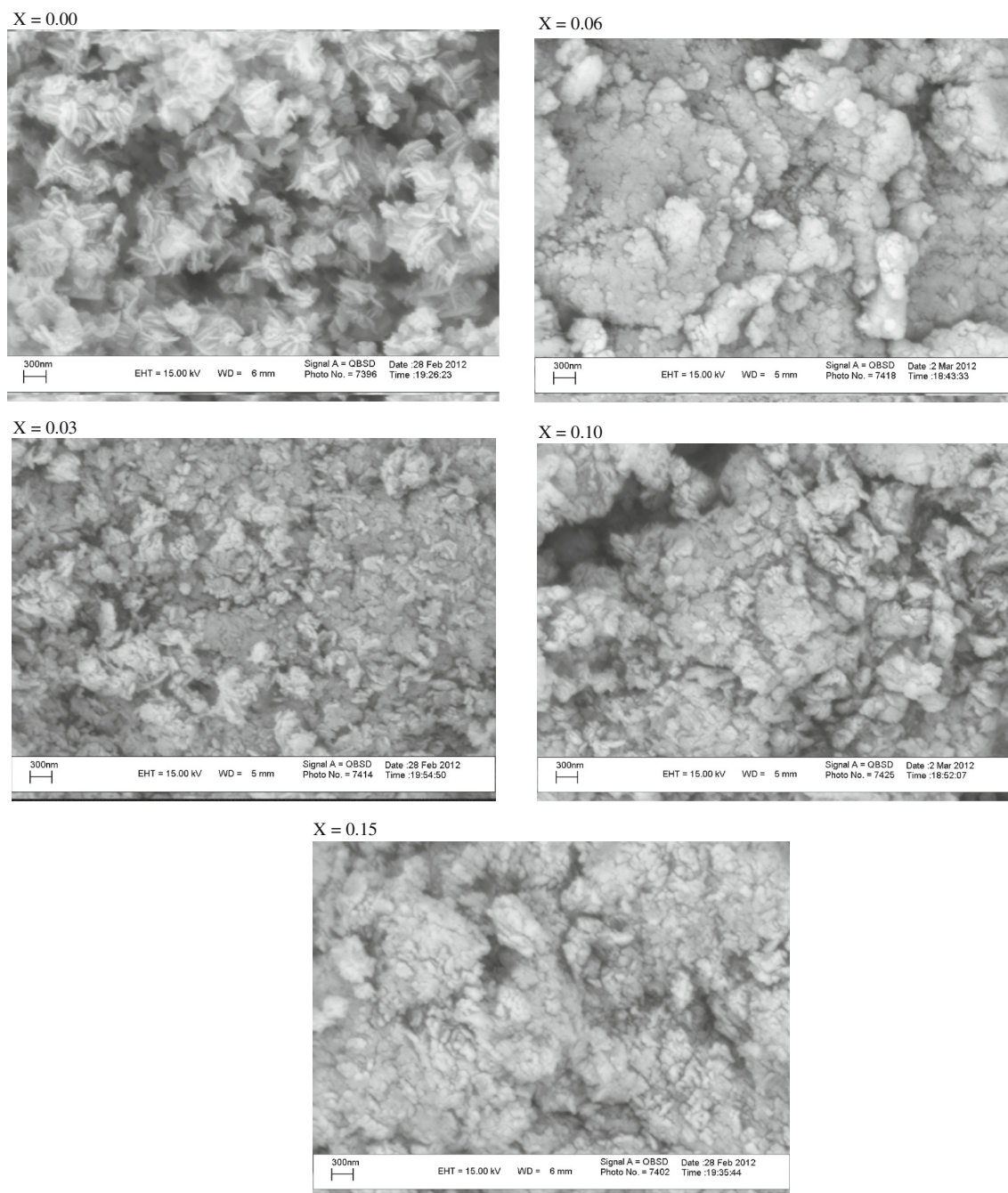


**Fig. 2** SEM images for Sb-doped ZnO nanostructures with various mole fractions of  $\text{Sb}^{+3}$  ions

0.15 mol fractions of  $\text{Sb}^{+3}$  ions are 0.028, 0.055, 0.092 and 0.138, respectively.

Photocatalytic activity of the nanostructures was investigated by degradation of MB, which is a typical dye resistant to biodegradation, under UV irradiation. In Fig. 6, plots for photodegradation of MB on the nanostructures are shown. As can be seen, all of the Sb-doped nanostructures exhibit higher activity than the pure ZnO. Among the nanostructures, the sample with 0.10 mol fraction of  $\text{Sb}^{+3}$  ions has highest activity.

Dependence of photocatalytic reaction rate on the concentration of MB as an organic pollutant is generally described by the following kinetic model [38]:

$$\text{rate} = -\frac{d[\text{MB}]}{dt} = \frac{kK[\text{MB}]}{1 + K[\text{MB}]} \quad (3)$$

where  $k$  is first-order rate constant of the reaction and  $K$  is adsorption constant of MB on the photocatalyst. Equation (3) can be simplified to a pseudo first-order equation [38]:

(a) for pure ZnO nanostructures



(b) for Sb-doped ZnO nanostructures

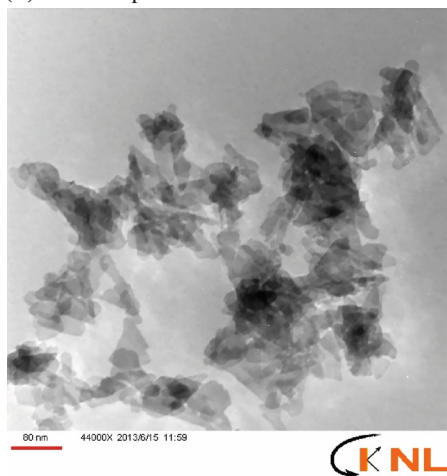


**Fig. 3** TEM images for **a** ZnO and **b** Sb-doped ZnO nanostructures with 0.1 mol fraction of the dopant

$$\ln \frac{[MB]_o}{[MB]} = \ln \frac{A_0}{A} = kKt = k_{obs}t \quad (4)$$

in which  $k_{obs}$  is observed first-order rate constant of the reaction. The rate constants for degradation of MB on Sb-doped ZnO nanostructures with 0.10 mol fraction of  $Sb^{+3}$  ions and pure ZnO are  $9.38 \times 10^{-2}$  and  $4.68 \times 10^{-2} \text{ min}^{-1}$ , respectively. Then, the degradation rate constant on the nanostructure increases nearly two times relative to the pure ZnO. As can be seen in Fig. 6, after irradiation for 30 min, degradation of MB on the Sb-doped ZnO and pure ZnO is 94.4 and 64.4 %, respectively.

To obtain maximum degradation efficiency, influence of various operational parameters including (1) microwave irradiation time, (2) calcination temperature, (3) catalyst weight, and (4) pH of solution on the degradation of MB was investigated and the results are discussed in the following sections.

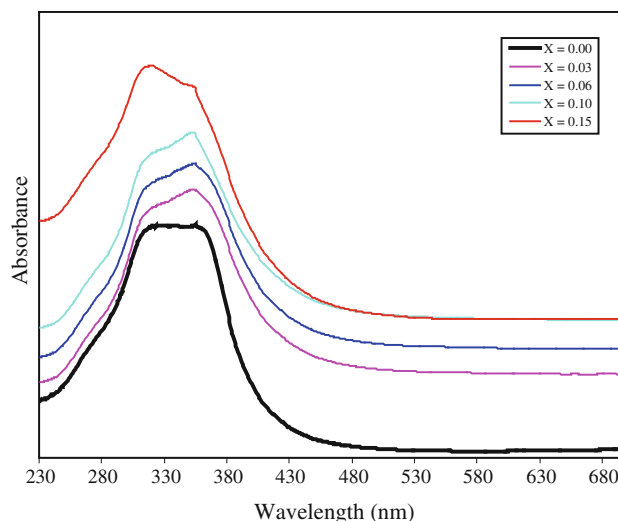


**Fig. 4** UV-vis DRS for Sb-doped ZnO nanostructures with various mole fractions of  $Sb^{+3}$  ions

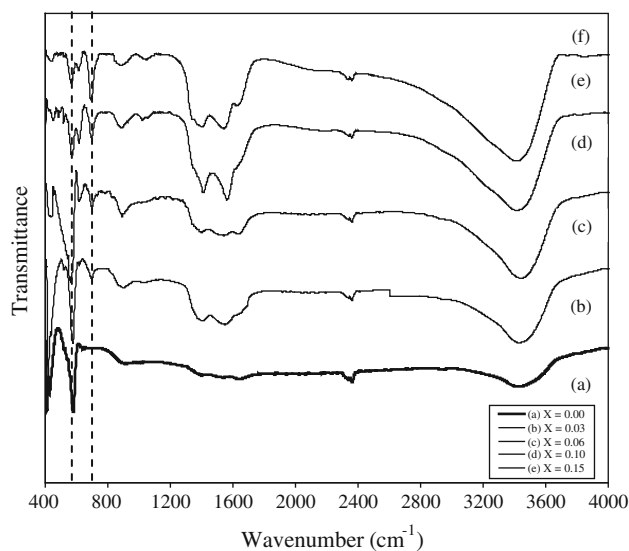


**Fig. 5** FT-IR spectra for Sb-doped ZnO nanostructures with various mole fractions of  $Sb^{+3}$  ions

#### Effect of microwave irradiation time

To study the influence of irradiation time applied for preparation of the nanostructures with 0.10 mol fraction of  $Sb^{+3}$  ions, four comparative samples were prepared, keeping the reaction parameters constant except that the nanostructures were prepared by microwave irradiations for 2.5, 5, 10 and 15 min. Plots for photocatalytic degradation of MB on the nanostructures prepared at various irradiation times are demonstrated in Fig. 7. As can be seen, the degradation reaction initially increases with irradiation time up to 5 min and then decreases. Enhancing the photocatalytic activity with increasing irradiation time can be attributed to increasing crystallinity of the

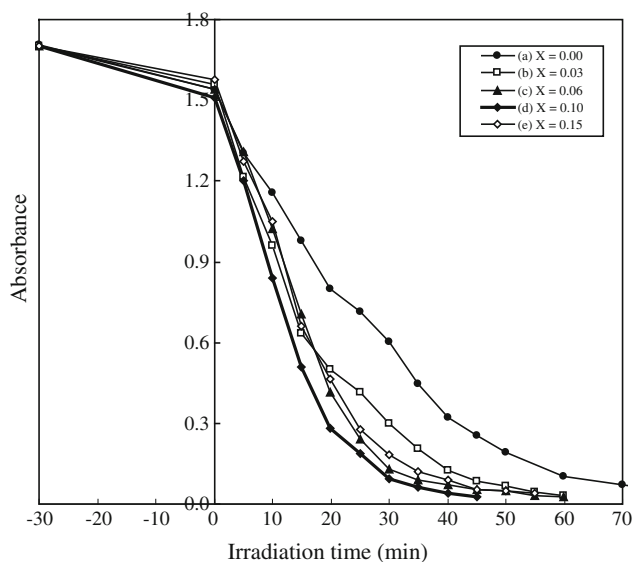


**Fig. 6** Photodegradation of MB under UV irradiation on Sb-doped ZnO nanostructures with various mole fractions of  $\text{Sb}^{+3}$  ions

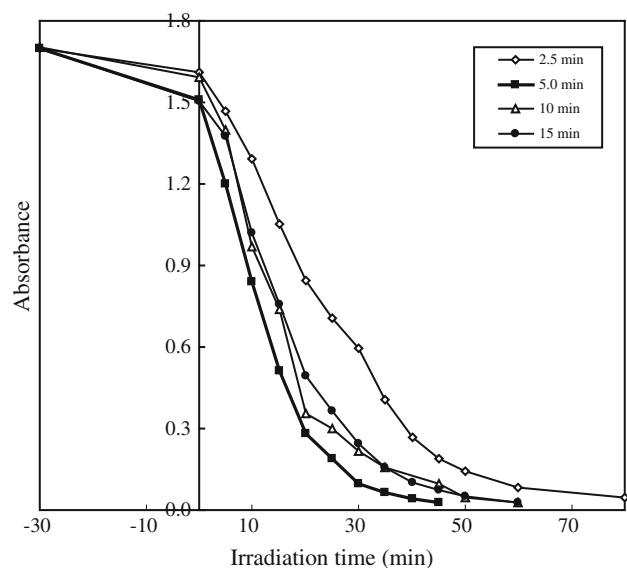


**Fig. 7** Photodegradation of MB on Sb-doped ZnO nanostructures prepared at various microwave irradiation times

nanostructures. Further irradiations can increase size and aggregation of the nanostructures and hence the photocatalytic activity will be decreased.

#### Effect of calcination temperature

It is well known that calcination temperature changes photocatalytic activity of nanomaterials. To investigate the effect of calcination temperature, degradation of MB on the nanostructures with 0.10 mol fraction of  $\text{Sb}^{+3}$  ions (prepared by 5 min microwave irradiation) calcinated for 2 h at

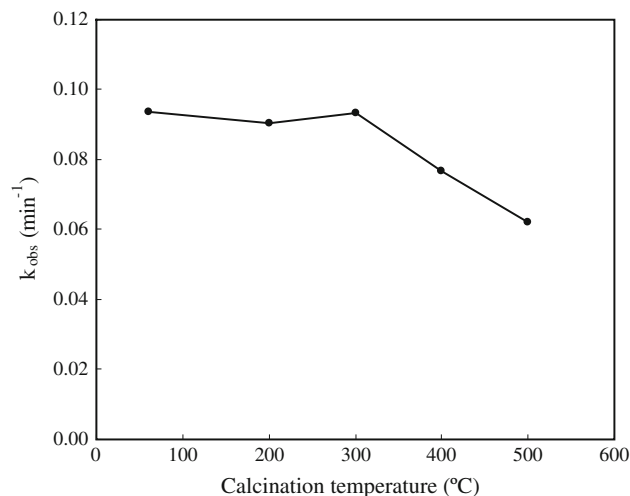


**Fig. 8** Plot of observed first-order rate constant of the degradation reaction on Sb-doped ZnO nanostructures versus calcinations temperature

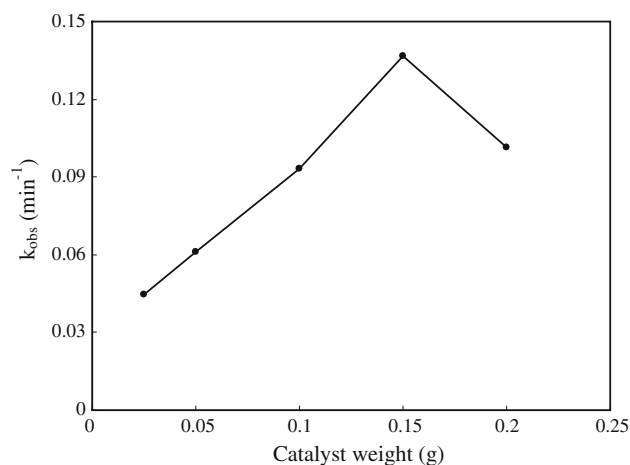


**Fig. 9** Plot of observed first-order rate constant of the degradation reaction on Sb-doped ZnO nanostructures versus catalyst weight

various temperatures is considered (Fig. 8). As can be seen, the degradation rate constant is nearly constant up to 300 °C and then decreases with further increasing calcination temperature. Decrease in the degradation rate constant is due to the aggregation of the nanostructures at higher temperatures [39].

#### Effect of the catalyst weight

To obtain the optimum catalyst weight, a series of experiments were carried out by changing weight of the nanostructures (prepared by 5 min microwave irradiation) between 0.025 and 0.20 g. In Fig. 9, the rate constant of the degradation reaction has been plotted versus weight of the photocatalyst. As can be seen, the rate constant increases with weight of the photocatalyst up to 0.15 g and then

decreases. With increasing weight of the photocatalyst, the active sites are increased. However, more photocatalyst would not only induce greater aggregation of the photocatalyst, but also increase scattering of light and reduce in light penetration through the solution [40].

#### Effect of solution pH

It is well known that pH of solutions influences adsorption and dissociation of substrate, photocatalyst surface charge and other physicochemical properties of system [41]. Then, pH of solution is an important variable in aqueous phase-mediated photocatalytic reactions. The effect of solution pH on the degradation reaction was studied by keeping all other experimental parameters constant and varying the initial pH between 2 and 13 (Fig. 10). As can be seen, the degradation reaction suddenly decreases with decreasing pH of the solution. Decrease in the degradation reaction in more acidic solutions can be attributed to dissolution of the nanostructures [39]. In these solutions, the photocatalyst has low stability and hence the degradation reaction is decreased at more acidic solutions. The zero point charge pH for the nanostructures will be about pH 9 [42]. Then, in various ranges of pH, there is electrostatic attraction or repulsion forces between surface of the nanostructures and MB, which consequently increase or decrease adsorption of the pollutant. Above zero point charge pH, surface of the photocatalyst will be negatively charged, then electrostatic attraction force between the negatively charged photocatalyst and MB (with positive charge) will lead to increased adsorption of MB. Therefore, degradation of MB on the nanostructures in solutions with pH 5–9 will be higher than those of more acidic and alkaline solutions.

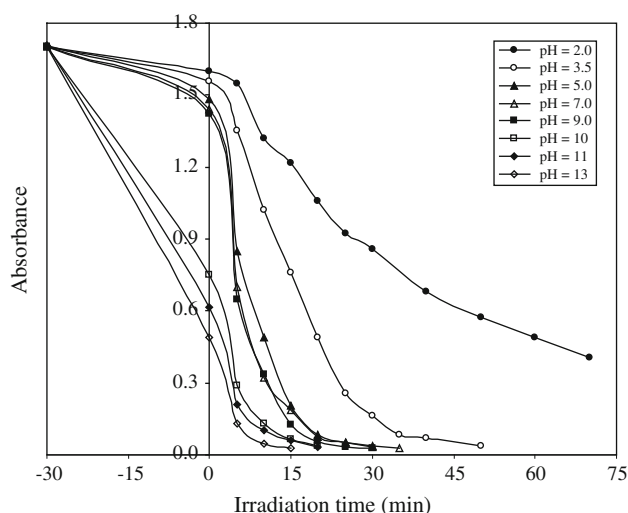


**Fig. 10** Photodegradation of MB on Sb-doped ZnO nanostructures at various pH

Very recently, we have prepared Sb-doped ZnO nanostructures by ultrasonic irradiation method at 60 min [43]. Preparation of the nanostructures by microwave irradiation has advantage of preparation in very short time (at 5 min). Moreover, after UV irradiation for 20 min, the degradation of MB on the nanostructures prepared by microwave and ultrasonic methods are 96.6 and 85 %, respectively. Therefore, the photocatalytic activity of the nanostructures prepared by microwave method is higher than that of the prepared photocatalyst by ultrasonic irradiation.

#### The photocatalyst reusability

Reusability of a photocatalyst is very important parameter to obtain a photocatalyst with high efficiency. To know reusability of the catalyst, the photodegradation experiments were carried out in optimized conditions (mole fraction of  $\text{Sb}^{+3}$  ions = 0.10, microwave irradiation time = 5 min, catalyst weight = 0.15 g and pH 5.4). The solution resulting from the photocatalytic degradation of MB was filtered, washed and the photocatalyst dried. The dried catalyst was used for the degradation reaction under similar conditions (Fig. 11). It can be seen that the degradation percent decreases to 82 % after four runs, indicating that the photocatalytic activity has a better reusability.

#### The degradation mechanism

After illumination of Sb-doped ZnO nanostructures with UV irradiation, electron–hole pairs are produced as the beginning of the degradation reactions. These photogenerated electron–hole pairs migrate to the surface of the nanostructures and undergo redox reactions with adsorbed MB molecules. But, recombination of the photogenerated

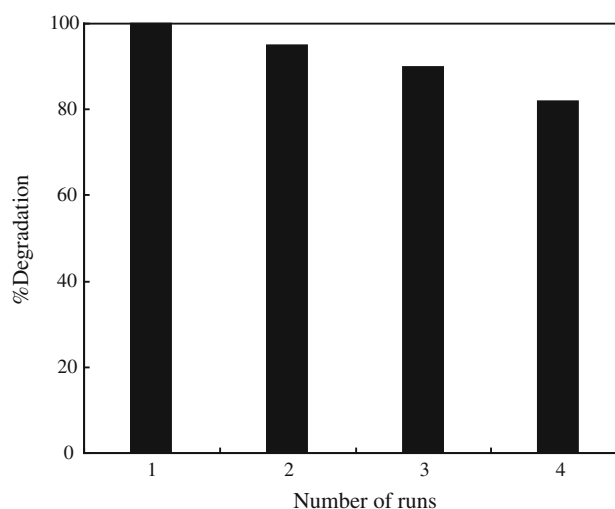
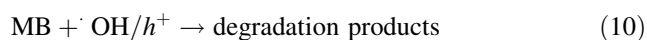
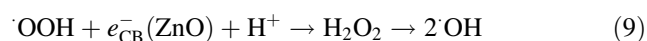
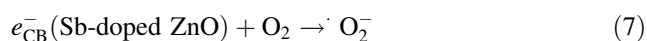
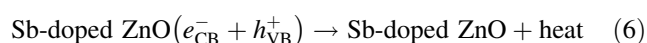
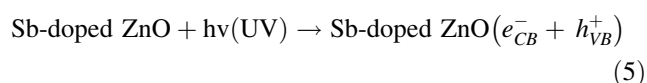


**Fig. 11** Plot of degradation % for MB on the nanostructures at optimized conditions versus number of runs

charge carriers is competing with the degradation reactions. It is well known that an important method for increasing photocatalytic activity is to suppress recombination of photogenerated electrons and holes to maximize the number of photogenerated electron–hole pairs [44]. Average diffusion time for the charge carriers to migrate from bulk to surface is calculated by  $r^2\pi^2D$ , where  $r$  and  $D$  are the grain radius and diffusion coefficient of charge carriers, respectively [45]. Then, for Sb-doped ZnO nanostructures with smaller size than the ZnO nanostructures, the diffusion time will be lower and hence the photogenerated electron–hole pairs easily reached to the surface of the nanostructures to react with adsorbed MB. Details of the degradation reactions can be summarized as follows:



By doping ZnO nanostructures with various cations, the trapping sites of charge carriers increase with increasing the amount of dopant concentration, which prolongs the lifetime of the carriers. For this reason, the photocatalytic degradation of MB on Sb-doped ZnO increases with mole fraction of  $\text{Sb}^{3+}$  ions. But, when the amount of  $\text{Sb}^{3+}$  ions is very high, the dopant ions can act as recombination centers of electrons and holes and hence the photocatalytic activity will be decreased [47]. Moreover, at higher mole fractions of  $\text{Sb}^{3+}$  ions, the charge carriers can be trapped more than once on their way to the surface so they recombine before they can reach to surface of the nanostructures. Therefore, higher activity of the doped nanostructures with optimum content of  $\text{Sb}^{3+}$  ions under UV irradiation is attributed to decreasing electron–hole recombination rate due to the separation of these pairs.

## Conclusions

Microwave irradiation method was applied for preparation of Sb-doped ZnO nanostructures ( $0 \leq$  mole fraction of  $\text{Sb}^{3+} \leq 0.15$ ) in water. This environmentally benign green method is template-free which remarkably shortens preparation time and avoids the complicated procedures. Doping of the ZnO nanostructures with 0.10 mol fraction of  $\text{Sb}^{3+}$  ions increases the degradation rate constant of MB about two times. The rate constant increases with weight of

the photocatalyst up to 0.15 g and then decreases. At higher calcination temperatures, the photocatalyst loses the active surface area and hence the photocatalytic activity decreases. Moreover, the reaction rate constant in acidic and alkaline solutions is lower than the neutral conditions. The photocatalyst retains 82 % of its activity after four cycles.

**Acknowledgments** The Authors wish to acknowledge University of Mohaghegh Ardabili, for financial support of this work.

## References

1. S. Barth, F. Hernandez-Ramirez, J.D. Holmes, A. Romano-Rodriguez, Synthesis and applications of one-dimensional semiconductors. *Prog. Mater. Sci.* **55**, 563–627 (2010)
2. X. Fang, T. Zhai, U.K. Gautam, L. Li, L. Wu, Y. Bando, D. Golberg, ZnS nanostructures: from synthesis to applications. *Prog. Mater. Sci.* **56**, 175–287 (2011)
3. K. Nakata, A. Fujishima,  $\text{TiO}_2$  photocatalysis: design and applications. *J. Photochem. Photobiol. C Photochem. Rev.* **13**, 169–189 (2012)
4. S.K. Arya, S. Saha, J.E. Ramirez-Vick, V. Gupta, S. Bhansali, S.P. Singh, Recent advances in ZnO nanostructures and thin films for biosensor applications: review. *Anal. Chim. Acta.* **737**, 1–21 (2012)
5. Y. Jiang, Y. Liu, L. Yang, J. Liu, Y. Lin, Ionic liquid assisted sol-gel prepared Ce-doped ZnO. *Adv. Mater. Res.* **490**, 3262–3265 (2012)
6. L. Zhang, Y.-J. Zhu, ZnO micro- and nano-structures: microwave-assisted solvothermal synthesis, morphology control and photocatalytic properties. *Appl. Phys. A* **97**, 847–852 (2009)
7. R. Jalal, E.K. Goharshadi, M. Abareshi, M. Moosavi, A. Yousefi, P. Nancarrow, ZnO nanofluids: green synthesis, characterization, and antibacterial activity. *Mater. Chem. Phys.* **121**, 198–201 (2010)
8. R. Kitture, S.L. Koppikar, R. Kaul-Ghanekar, S.N. Kale, Catalyst efficiency, photostability and reusability study of submicron sized ZnO particles in visible light for dye degradation. *J. Phys. Chem. Solids* **72**, 60–66 (2011)
9. A.B. Djurišić, A.M.C. Ng, X.Y. Chen, ZnO nanostructures for optoelectronics: material properties and device applications. *Prog. Quantum Electron.* **34**, 191–259 (2010)
10. L. Li, T. Zhai, Y. Bando, D. Golberg, Recent progress of one-dimensional ZnO nanostructured solar cells. *Nano Energy* **1**, 91–106 (2012)
11. A. Moezzi, A.M.M. Donagh, M.B. Cortie, Zinc oxide particles: synthesis, properties and applications. *Chem. Eng. J.* **185–186**, 1–22 (2012)
12. L. Schmidt-Mende, J.L. MacManus-Driscoll, ZnO-nanostructures, defects, and devices. *Mater. Today* **10**, 40–48 (2007)
13. A. Wei, L. Pan, W. Huang, Recent progress in the ZnO nanostructure-based sensors. *Mater. Sci. Eng. B* **176**, 1409–1421 (2011)
14. M. Fu, Y. Li, S. Wu, P. Lu, J. Liu, F. Dong, Sol-gel preparation and enhanced photocatalytic performance of Cu-doped ZnO nanoparticles. *Appl. Surf. Sci.* **258**, 1587–1591 (2011)
15. S. Dong, K. Xu, J. Liu, H. Cui, Photocatalytic performance of ZnO: Fe array films under sunlight irradiation. *Phys. B* **406**, 3609–3612 (2011)
16. H.H. Mohamed, D.W. Bahnemann, The role of electron transfer in photocatalysis: fact and fictions. *Appl. Catal. B Environ.* **128**, 91–104 (2012)



17. X. Fang, J. Li, D. Zhao, B. Li, Z. Zhang, D. Shen, X. Wang, Z. Wei, Structural and photoluminescence properties of aligned Sb-doped ZnO nanocolumns synthesized by the hydrothermal method. *Thin Solid Films* **518**, 5687–5689 (2010)
18. H. Benelmadjat, N. Touka, B. Harieche, B. Boudine, O. Halimi, M. Sebais, Study of structural and optical properties of Sb-doped ZnO thin films deposited by spin coating method. *Opt. Mater.* **32**, 764–767 (2010)
19. I.A. Palani, D. Nakamura, K. Okazaki, M. Higashihata, T. Okada, Influence of Sb as a catalyst in the growth of ZnO nano wires and nano sheets using nanoparticle assisted pulsed laser deposition (NAPLD). *Mater. Sci. Eng. B* **176**, 1526–1530 (2011)
20. C.H. Zhang, J.F. Su, B. Wang, D.M. Zhang, Y.S. Zhang, Photoluminescence of ZnO: Sb nanobelts fabricated by thermal evaporation method. *J. Lumin.* **131**, 1817–1820 (2011)
21. I.A. Palani, K. Okazaki, D. Nakamura, K. Sakai, M. Higashihata, T. Okada, Influence of Sb in synthesise of ZnO nanowire using sandwich type substrate in carbothermal evaporation method. *Appl. Surf. Sci.* **258**, 3611–3616 (2012)
22. S.B. Rana, A. Singh, N. Kaur, Structural and optoelectronic characterization of prepared and Sb-doped ZnO nanoparticles. *J. Mater. Sci. Mater. Electron.* **24**, 44–52 (2013)
23. M. Abaker, A. Umar, S.A. Al-Sayari, G.N. Dar, M. Faisal, S.H. Kim, S.W. Hwang, Growth and photocatalytic properties of Sb-doped ZnO nanoneedles by hydrothermal process. *AIP Conf. Proc.* **1370**, 121–127 (2011)
24. J.M. Wu, C.-W. Fang, L.-T. Lee, H.-H. Yeh, Y.-H. Lin, P.-H. Yeh, L.-N. Tsai, L.-J. Lin, Photoresponsive and ultraviolet visible-light range photocatalytic properties of ZnO: Sb nanowires. *J. Electrochem. Soc.* **158**, 6–10 (2011)
25. B. Baruwati, V. Polshettiwar, R.S. Varma, Microwave-assisted synthesis of nanomaterials in aqueous media, in *Aqueous microwave assisted chemistry, synthesis and catalysis*, ed. by V. Polshettiwar, R.S. Varma (RSC, UK, 2010), pp. 176–209
26. V. Polshettiwar, R.S. Varma, Fundamentals of aqueous microwave chemistry, in *Aqueous microwave assisted chemistry, synthesis and catalysis*, ed. by V. Polshettiwar, R.S. Varma (RSC, UK, 2010), pp. 1–8
27. D.-M. Gu, Y.-Y. Chu, Z.-B. Wang, Z.-Z. Jiang, G.-P. Yin, Y. Liu, Methanol oxidation on Pt/CeO<sub>2</sub>-C electrocatalyst prepared by microwave-assisted ethylene glycol process. *Appl. Catal. B Environ.* **102**, 9–18 (2011)
28. N. Uma Sangari, S. Chitra Devi, Synthesis and characterization of nano ZnO rods via microwave assisted chemical precipitation method. *J. Solid State Chem.* **197**, 483–488 (2013)
29. W. Shi, Y. Yan, X. Yan, Microwave-assisted synthesis of nanoscale BiVO<sub>4</sub> photocatalysts and their excellent visible-light-driven photocatalytic activity for the degradation of ciprofloxacin. *Chem. Eng. J.* **215–216**, 740–746 (2013)
30. B.G. Mishra, G.R. Rao, Promoting effect of ceria on the physicochemical and catalytic properties of CeO<sub>2</sub>-ZnO composite oxide catalysts. *J. Mol. Catal. A Chem.* **243**, 204–213 (2006)
31. B.D. Cullity, *Elements of X-ray diffraction*, 2nd edn. (Addison Wesley, London, 1978)
32. Y. Ao, J. Xu, D. Fu, X. Shen, C. Yuan, Low temperature preparation of anatase TiO<sub>2</sub>-coated activated carbon. *Colloids Surf. A Physicochem. Eng. Aspects* **312**, 125–130 (2008)
33. K.C. Barick, S. Singh, M. Aslam, D. Bahadur, Porosity and photocatalytic studies of transition metal doped ZnO nanoclusters. *Microporous Mesoporous Mater.* **134**, 195–202 (2010)
34. Q. Shi, J. Zhang, D. Zhang, C. Wang, B. Yang, B. Zhang, W. Wang, Red luminescent and structural properties of Mg-doped ZnO phosphors prepared by sol-gel method. *Mater. Sci. Eng. B* **177**, 689–693 (2012)
35. L.I. Berger, *Semiconductor materials* (CRC, Boca Raton, 1997)
36. M. Barzegar, A. Habibi-Yangjeh, M. Behboudnia, Template-free preparation and characterization of nanocrystalline ZnO in aqueous solution of [EMIM][EtSO<sub>4</sub>] as a low-cost ionic liquid using ultrasonic irradiation and photocatalytic activity. *J. Phys. Chem. Solids* **70**, 1353–1358 (2009)
37. A.H. Abdullah, N.H.M. Noor, I. Ramli, Effect of precipitation route on the properties of antimony trioxide. *Mater. Chem. Phys.* **11**, 201–204 (2008)
38. M.A. Behnajady, N. Modirshahla, R. Hamzavi, Kinetic study on photocatalytic degradation of CI Acid Yellow 23 by ZnO photocatalyst. *J. Hazard. Mater. B* **133**, 226–232 (2006)
39. E. Sanatgar-Delshade, A. Habibi-Yangjeh, M. Khodadadi-Moghaddam, Hydrothermal and low temperature preparation and characterization of ZnO nanoparticles supported on natural zeolite as a highly efficient photocatalyst. *Monatsh. Chem.* **142**, 119–129 (2011)
40. N. Daneshvar, D. Salari, A.R. Khataee, The effect of operational parameters on the photocatalytic degradation of acid red 18 by ZnO. *J. Photochem. Photobiol. A Chem* **157**, 111–116 (2003)
41. M.V. Shankar, S. Anandan, N. Venkatachalam, B. Arabindoo, V. Murugesan, Novel thin-film reactor for photocatalytic degradation of pesticides in an aqueous solution. *J. Chem. Technol. Biotechnol.* **79**, 1279–1285 (2004)
42. N. Sobana, M. Swaminathan, The effect of operational parameters on the photocatalytic degradation of acid red 18 by ZnO. *Sep. Purif. Technol.* **56**, 101–107 (2007)
43. A. Omid, A. Habibi-Yangjeh, M. Pirhashemi, Application of ultrasonic irradiation method for preparation of ZnO nanostructures doped with Sb<sup>+3</sup> ions as a highly efficient photocatalyst. *Appl. Surf. Sci.* **276**, 468–475 (2013)
44. D. Robert, Photosensitization of TiO<sub>2</sub> by MxOy and MxSy nanoparticles for heterogeneous photocatalysis applications. *Catal. Today* **122**, 20–26 (2007)
45. M. Shang, W. Wang, S. Sun, L. Zhou, L. Zhang, Bi<sub>2</sub>WO<sub>6</sub> nanocrystals with high photocatalytic activities under visible light. *J. Phys. Chem. C* **112**, 10407–10411 (2008)
46. A.L. Stroyuk, A.I. Kryukov, S.Y. Kuchmii, V.D. Pokhodenko, Quantum size effects in semiconductor photocatalysis. *Theor. Exp. Chem.* **41**, 207–228 (2005)
47. S. Sakthivel, B. Neppolian, M.V. Shankar, B. Arabindoo, M. Palanichamy, V. Murugesan, Solar photocatalytic degradation of azo dye: comparison of photocatalytic efficiency of ZnO and TiO. *Sol. Energy Mater. Sol. Cells* **77**, 65–82 (2003)